Radiation defect data for a Virtual Tokamak Reactor model

S.L. Dudarev

CCFE, Culham Science Centre, Oxfordshire, UK

Integrated model for a tokamak reactor

UK Atomic Energy Authority

Plasma as a 3D neutron source

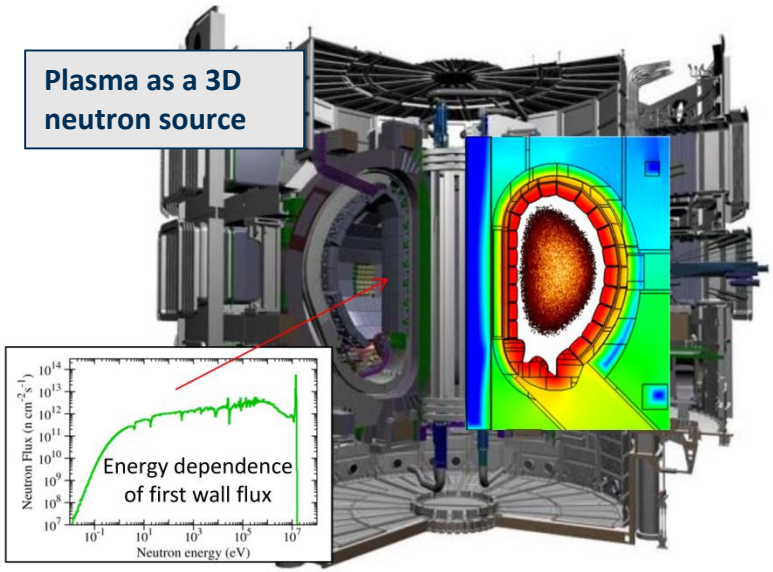

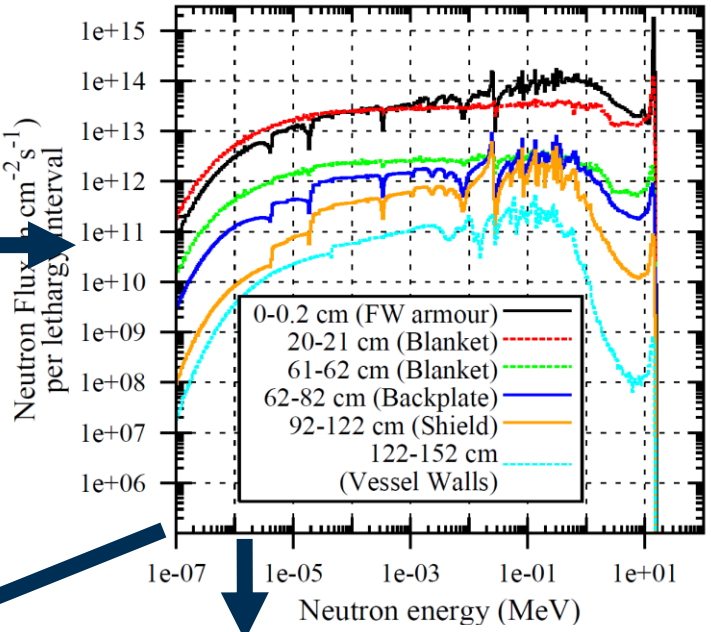

Neutron spectra at various locations in a DEMO power plant

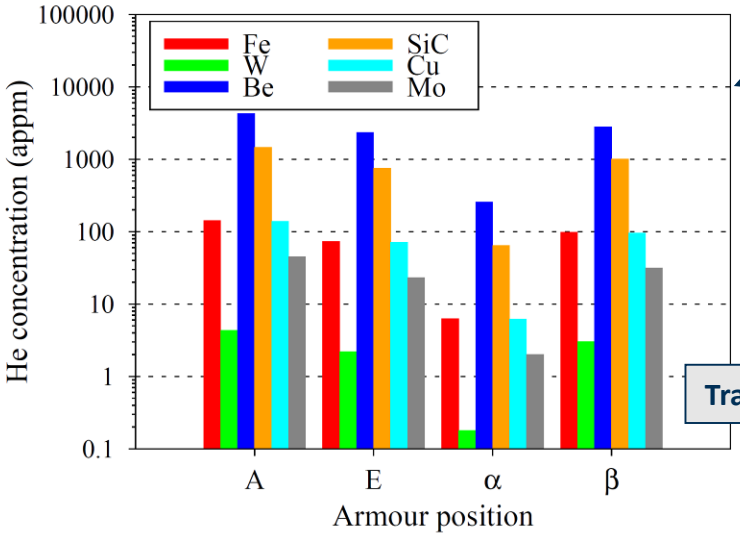

Transmutations

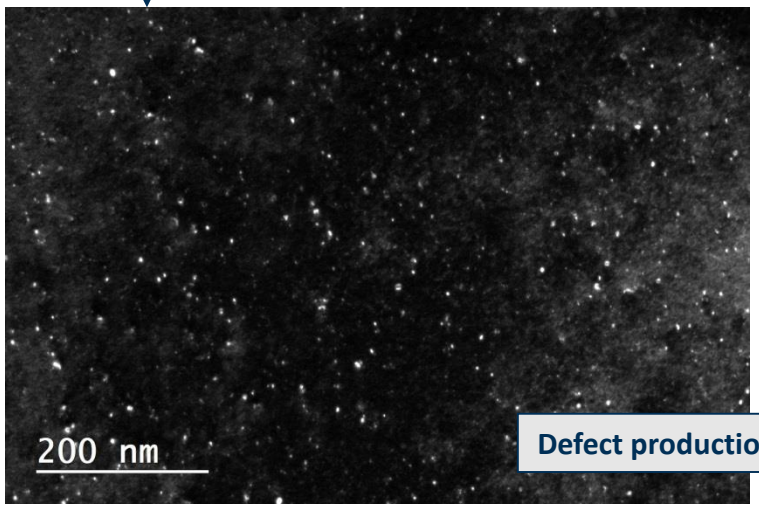

Defect production

M.R. Gilbert *et al.*, Nucl. Fusion **52** (2012) 083019; J. Nucl. Mater. **442** (2013) S755; J. Nucl. Mater. **467** (2015) 121; Nucl. Fusion **57** (2017) 044002

Transmutations: fission vs fusion

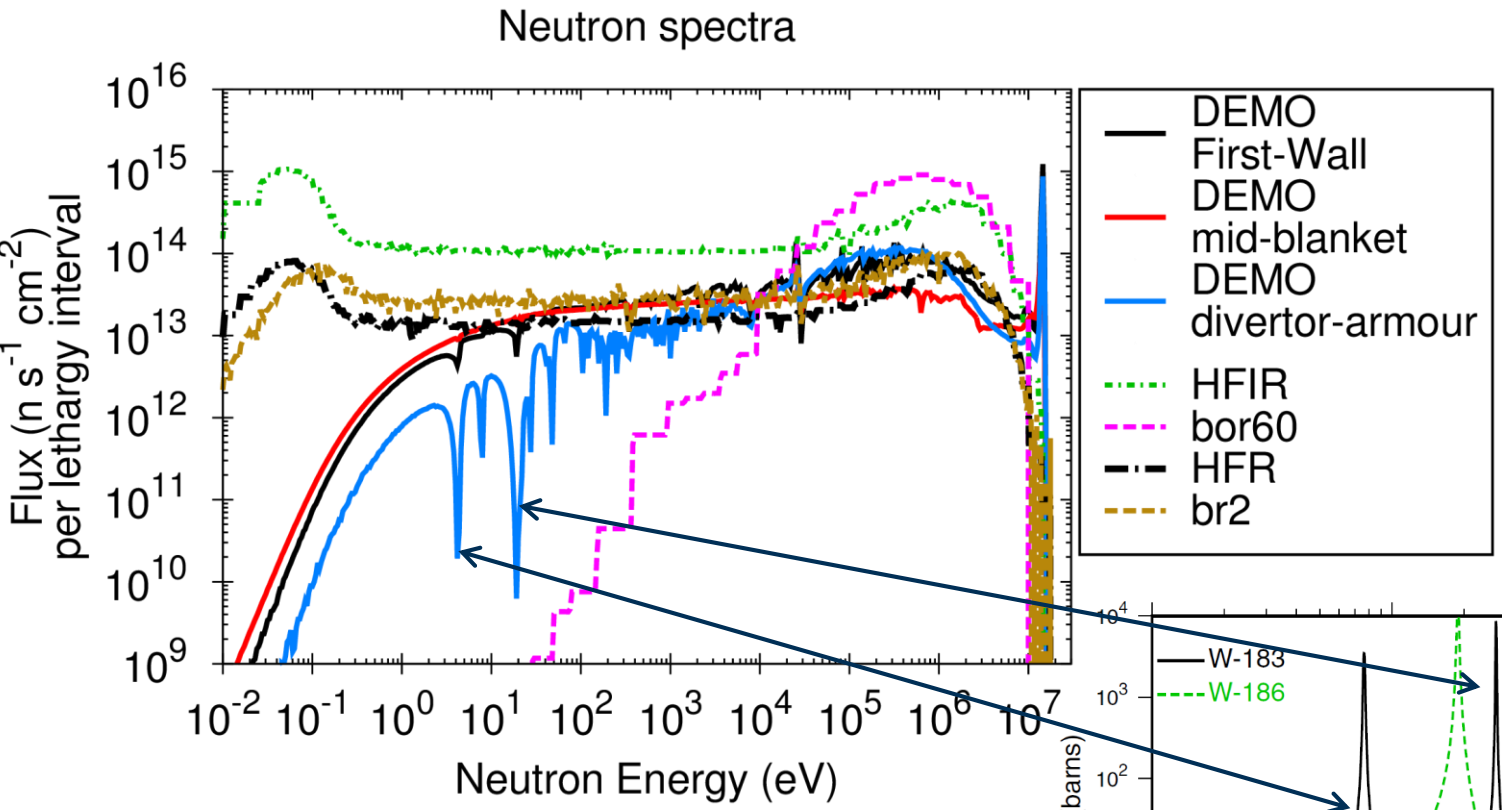

Note the enhanced low energy part of n-spectra in fission reactors.

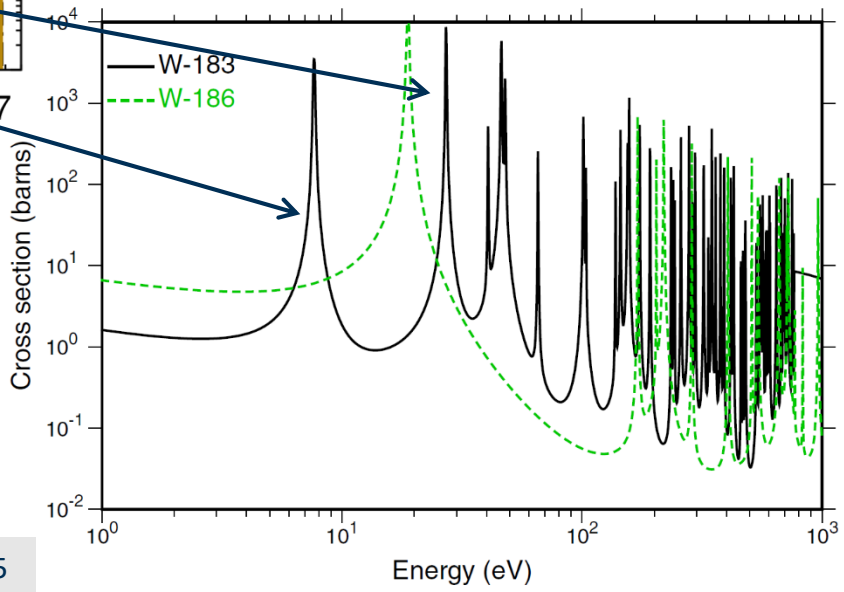

Minima in the neutron spectra correspond to resonances in the neutron absorption cross-section. Neutron absorption gives rise to transmutations.

M.R. Gilbert and J.-C. Sublet, Nuclear Fusion **51** (2011) 043005

Transmutations: fission vs fusion

UK Atomic Energy Authority

Fission

Water cooling problematic

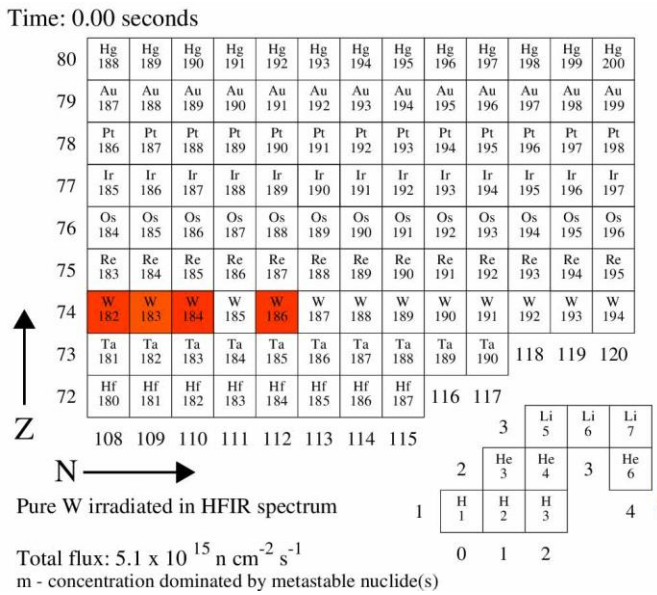

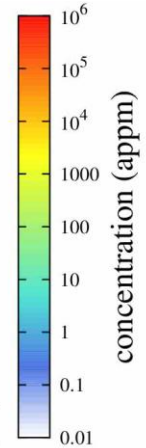

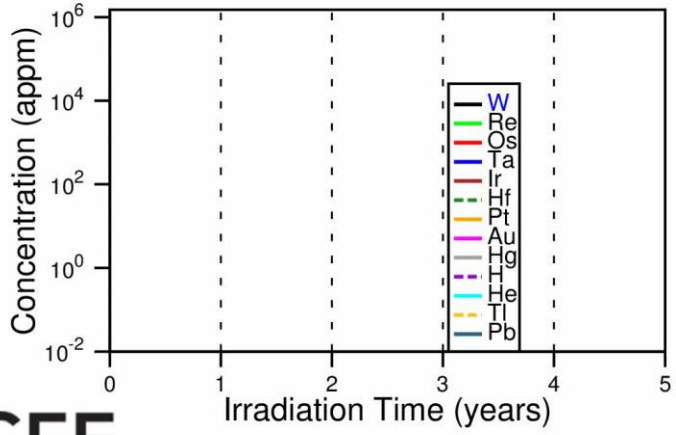

CCFE
CULHAM CENTRE FOR FUSION ENERGY

TUNGSTEN

Fusion

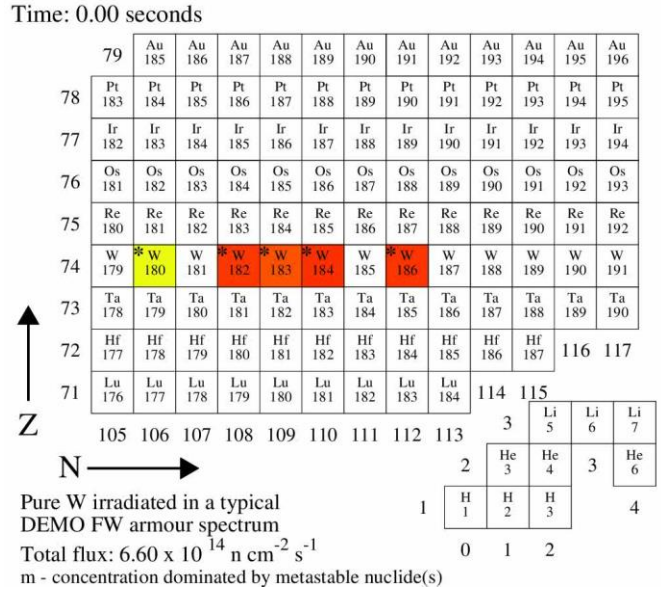

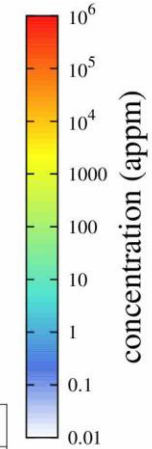

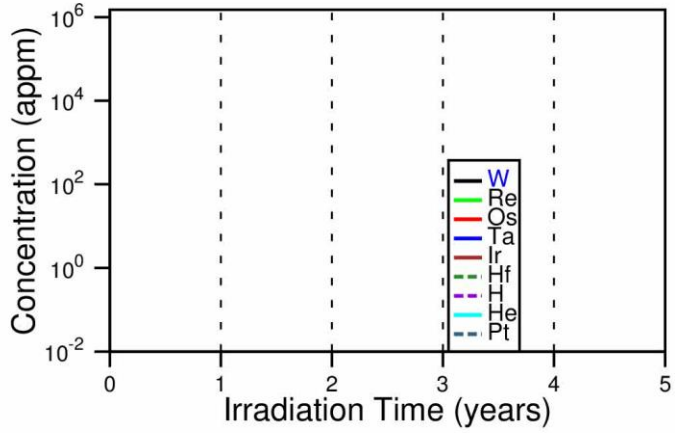

M.R. Gilbert and J.-C. Sublet, Nuclear Fusion **51** (2011) 043005;
M. R. Gilbert *et al.,* Nuclear Fusion **57** (2017) 044002

Production of radiation defects

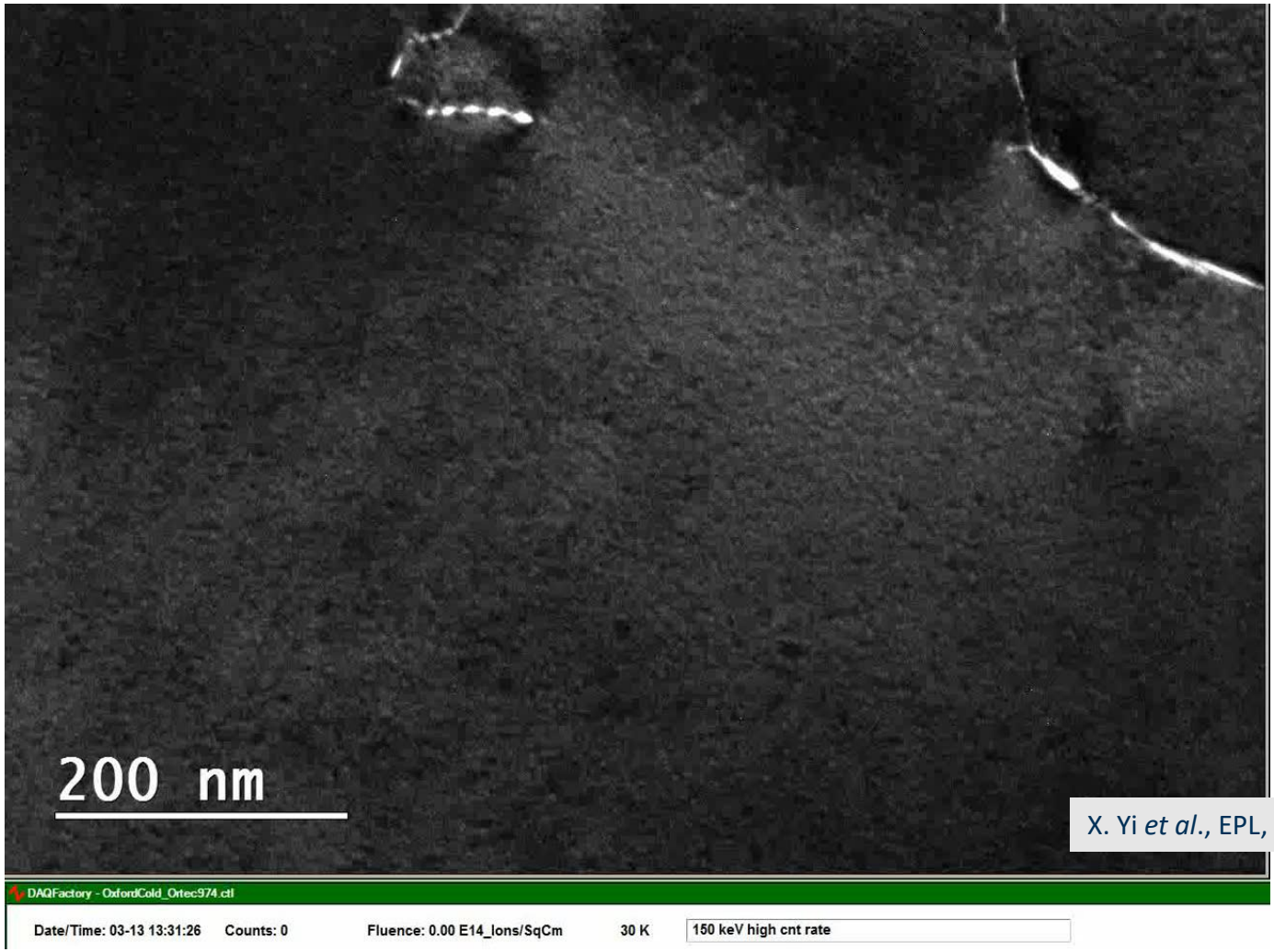

X. Yi *et al*., EPL, **110** (2015) 36001

In situ transmission electron microscope observation of accumulation of radiation damage in pure tungsten, bombarded by 150 keV W+ ions at 30K.

Invisible effects of irradiation

UK Atomic Energy Authority

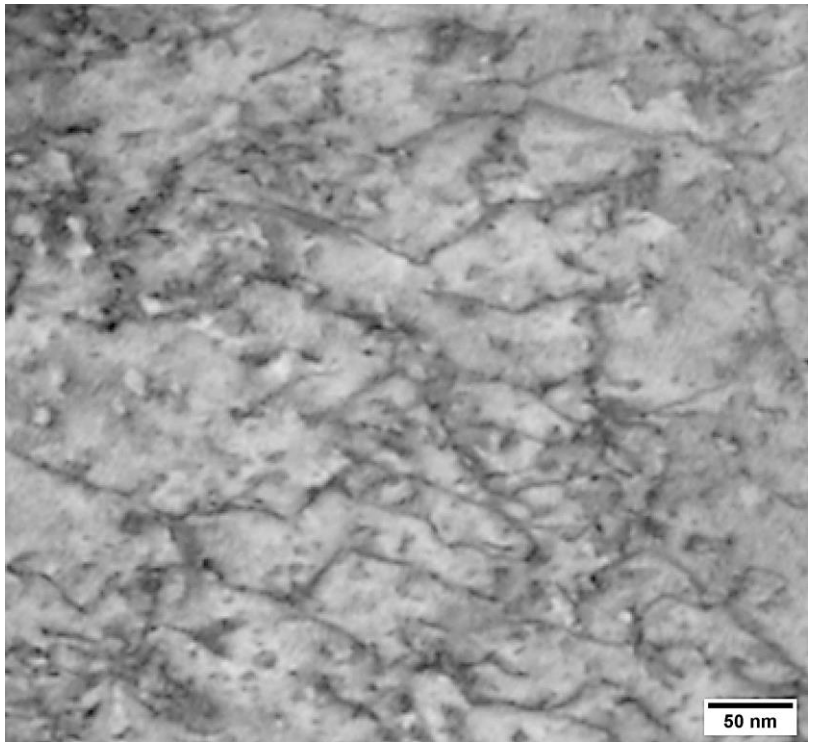

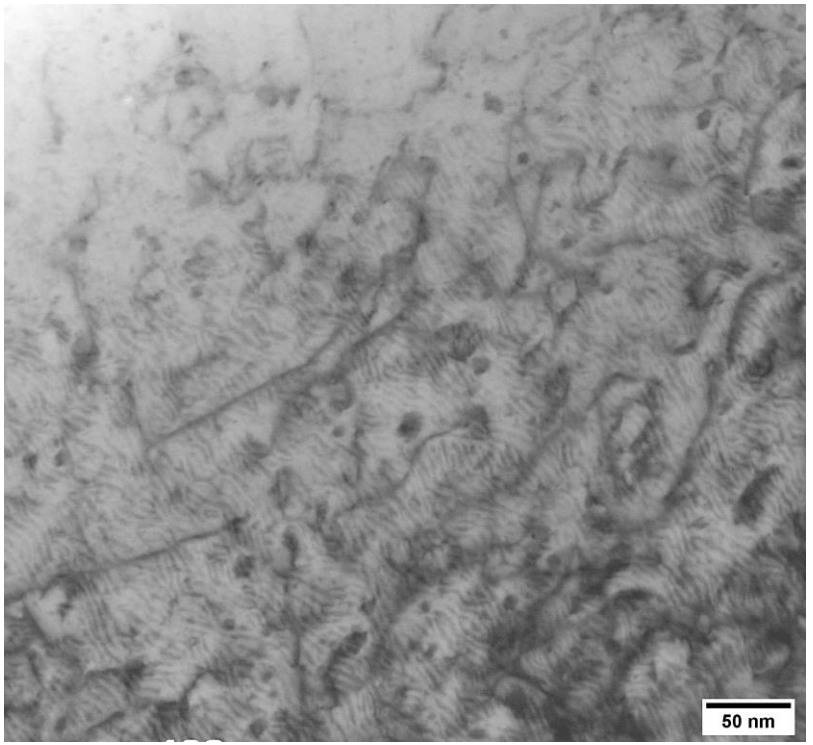

Comparison of electron microscope images of microstructure of unirradiated and irradiated, at 290 degrees C, F2W steel.

Neutron irradiated to 0.2 dpa

Unirradiated

Data courtesy of G.R. Odette and J. Haley, UCSB and Oxford

Invisible effects of irradiation

UK Atomic Energy Authority

X. Yi *et al.*, EPL **110** (2015) 36001

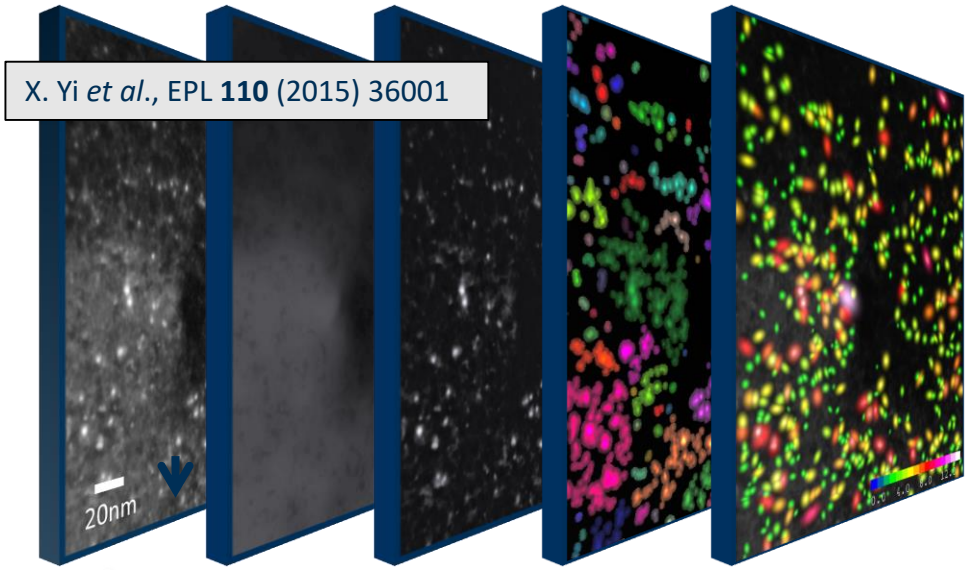

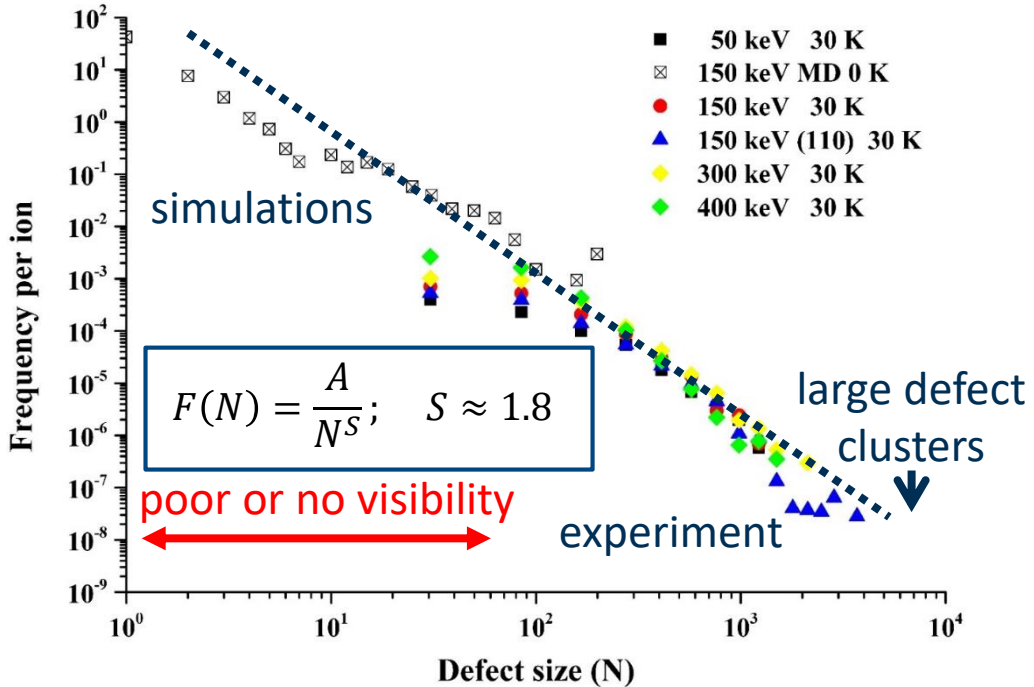

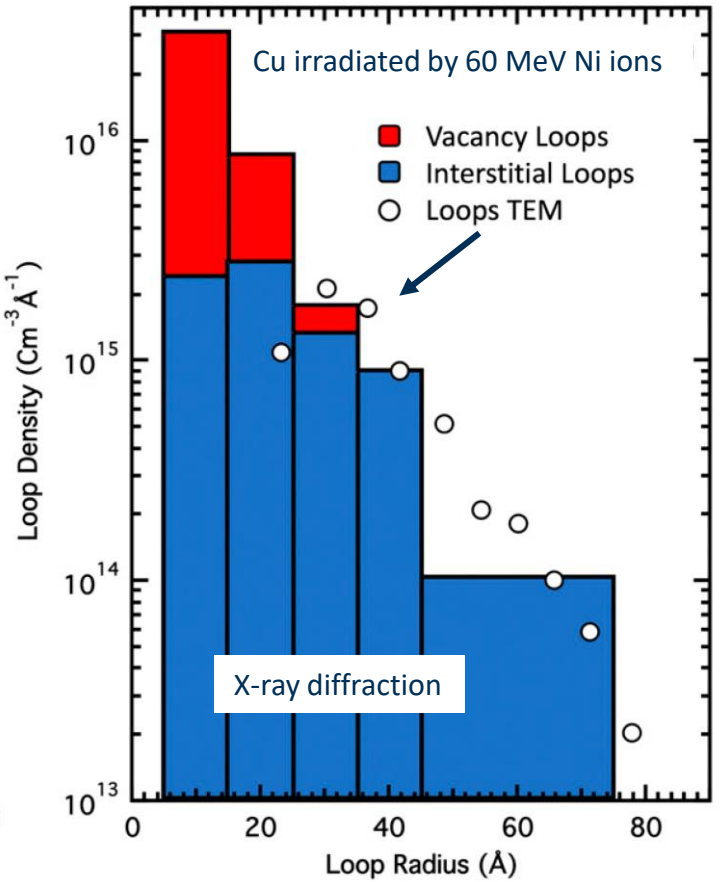

B.C. Larson, Crystals **9** (2019) 257

Strain from exposure to irradiation

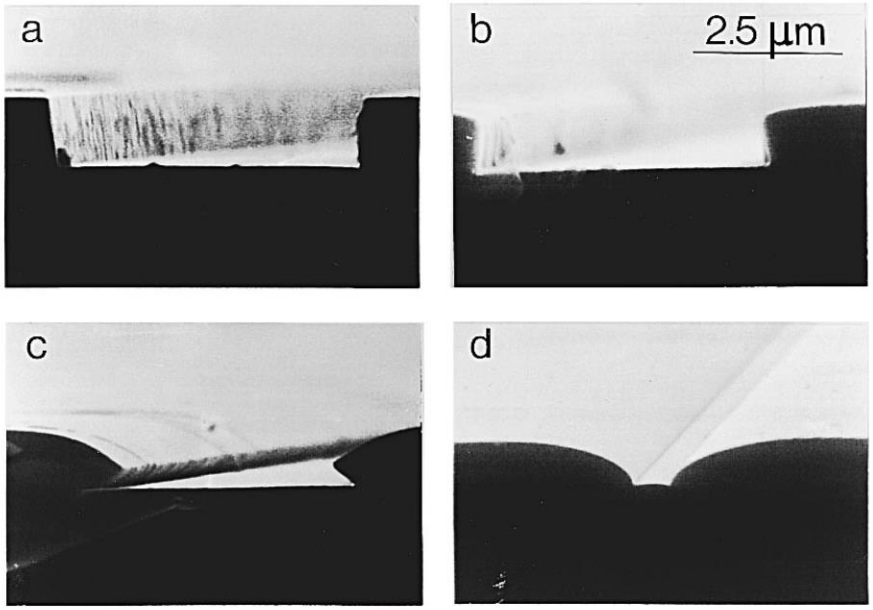

FIG. 1. Cross-section SEM images of a 5.0-μm-wide trench in a thermally grown SiO_2 film (a) before irradiation, and after 4.0 MeV Xe irradiation by (b) 1.0×10^{15}, (c) 3.0×10^{15}, and (d) $1.0\times10^{16}/cm^2$. All images were taken with the same magnification. The ion beam is directed perpendicular to the surface.

E. Snoeks *et al.*, Appl. Phys. Lett. **65** (1994) 2487

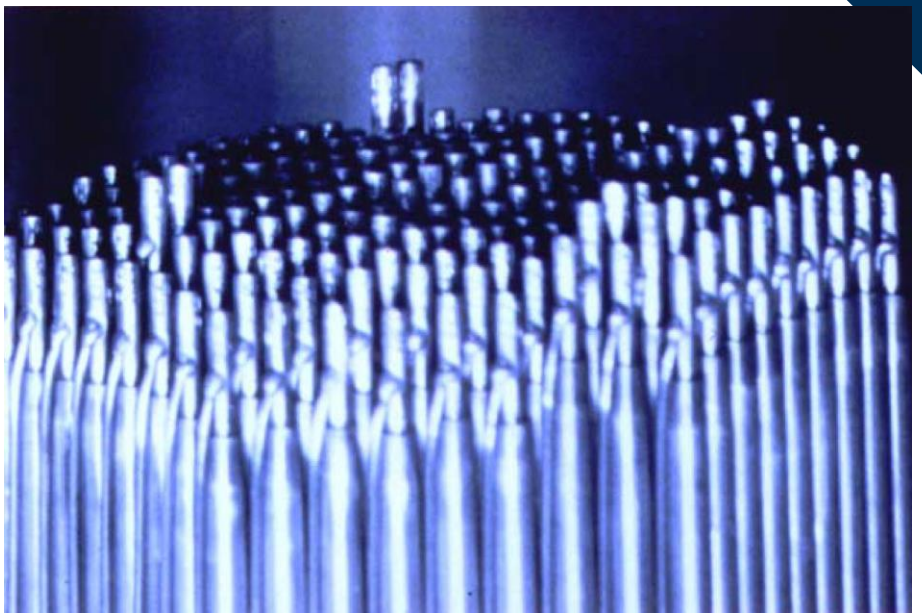

Dimensional changes in the stainless steel nuclear reactor components exposed to the neutron dose of ~ 75 dpa.

Courtesy of F. Garner (2006)

Strain from exposure to irradiation

UK Atomic Energy Authority

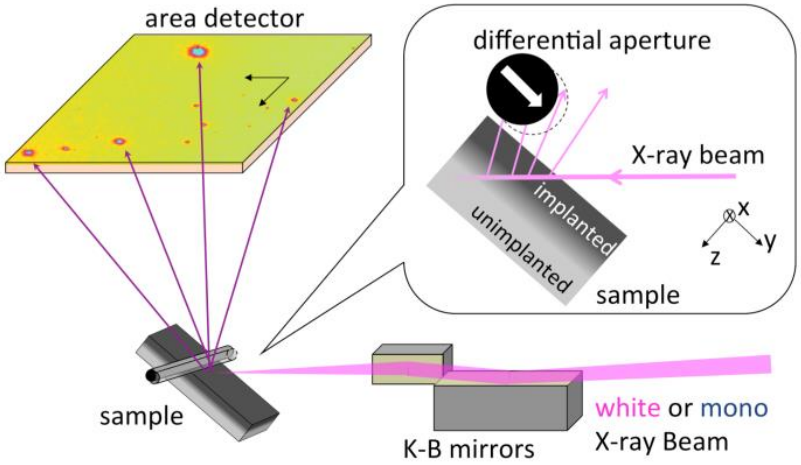

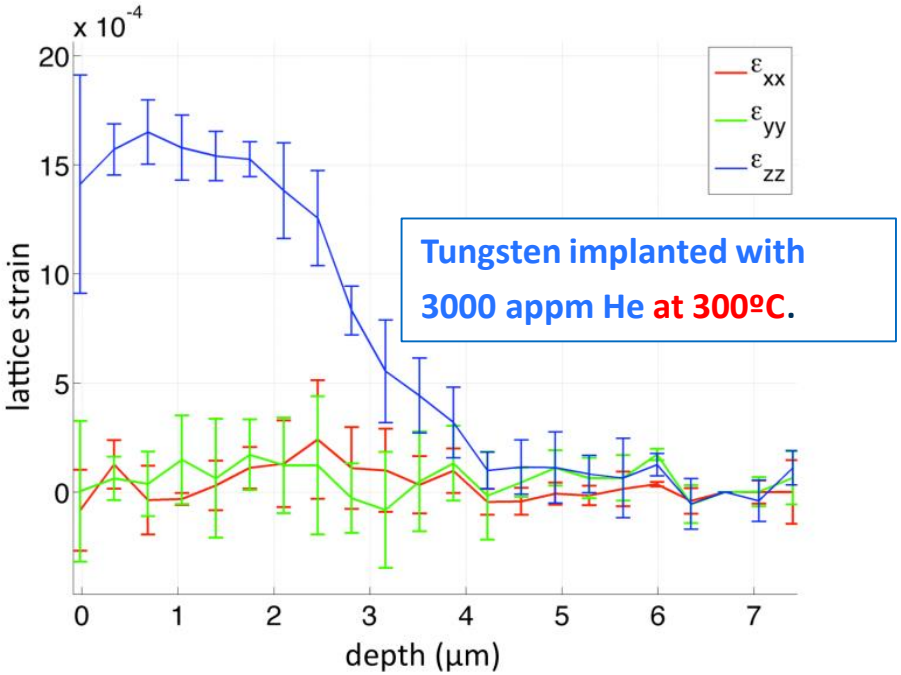

Tungsten implanted with 3000 appm He at 300ºC.

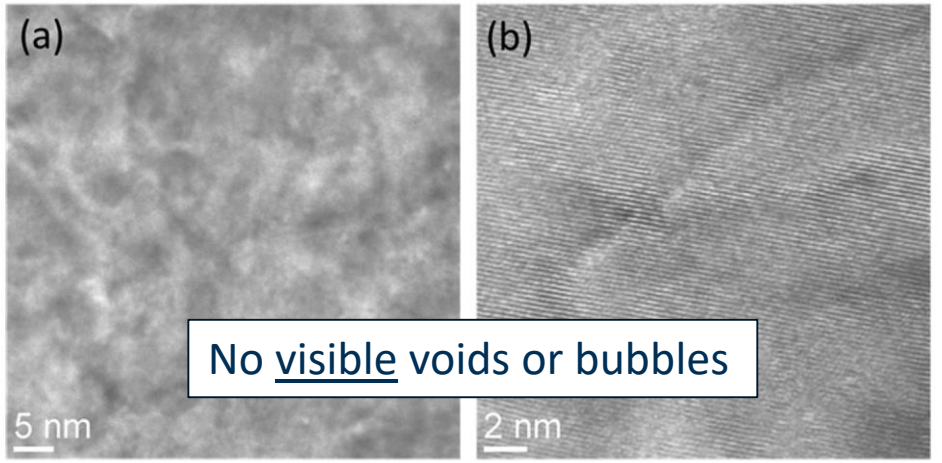

No visible voids or bubbles

FIG. 4. TEM micrographs of the 3000 appm He implanted pure W. The image was recorded at ~1 μm underfocus. No Fresnel contrast was observed in a through-focus series indicating no He bubbles are present.

Two possible modes of swelling:

- volume increase due to voids in the bulk and "redeposition"of atoms to the surface or grain boundaries.
- macroscopic strain due to local microscopic distortions from invisible atomic-scale defects.

F. Hofmann et al., Acta Materialia **89** (2015) 352

Neutron power density deposited in fusion blanket materials

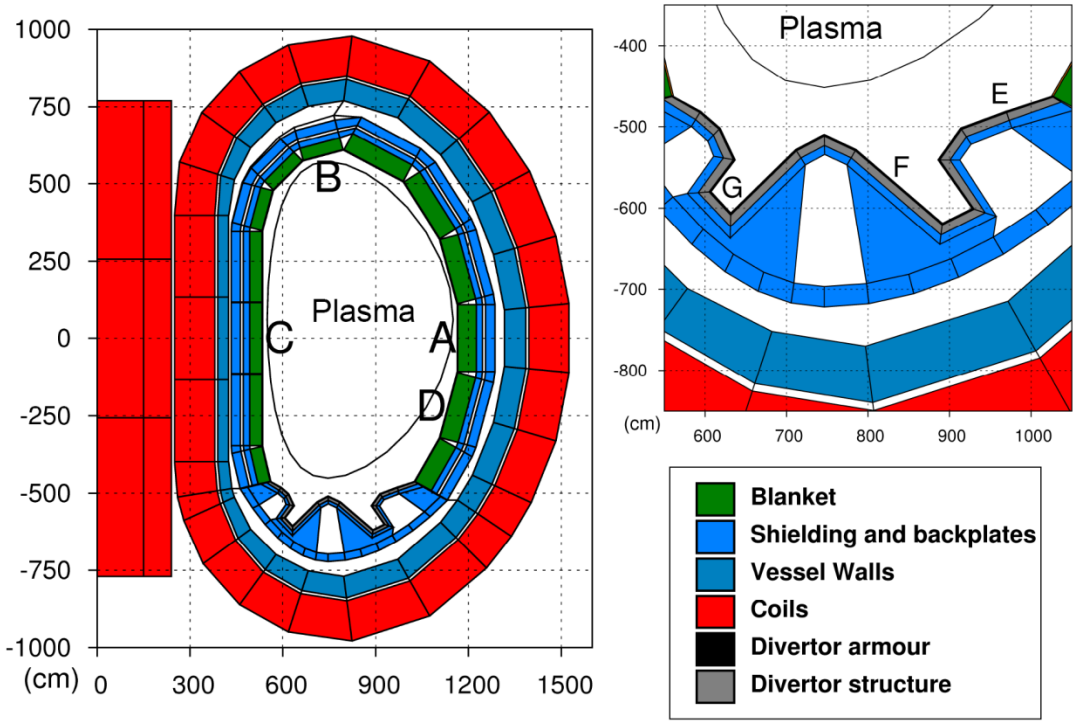

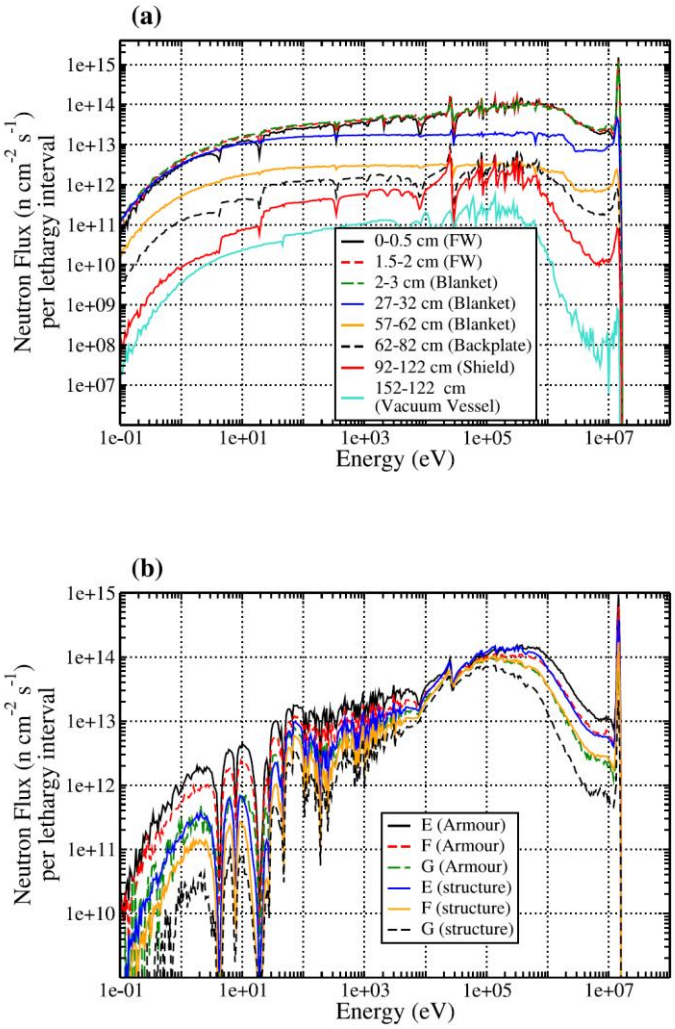

Above: a simplified model of DEMO used in neutron transport calculations. **Right**: (a) neutron energy spectra as functions of depth at the equatorial position and (b) at various positions in the divertor region.

M.R. Gilbert *et al*., Nucl. Fusion **52** (2012) 083019; J. Nucl. Mater. **442** (2013) S755

Neutron power density deposited in fusion blanket materials

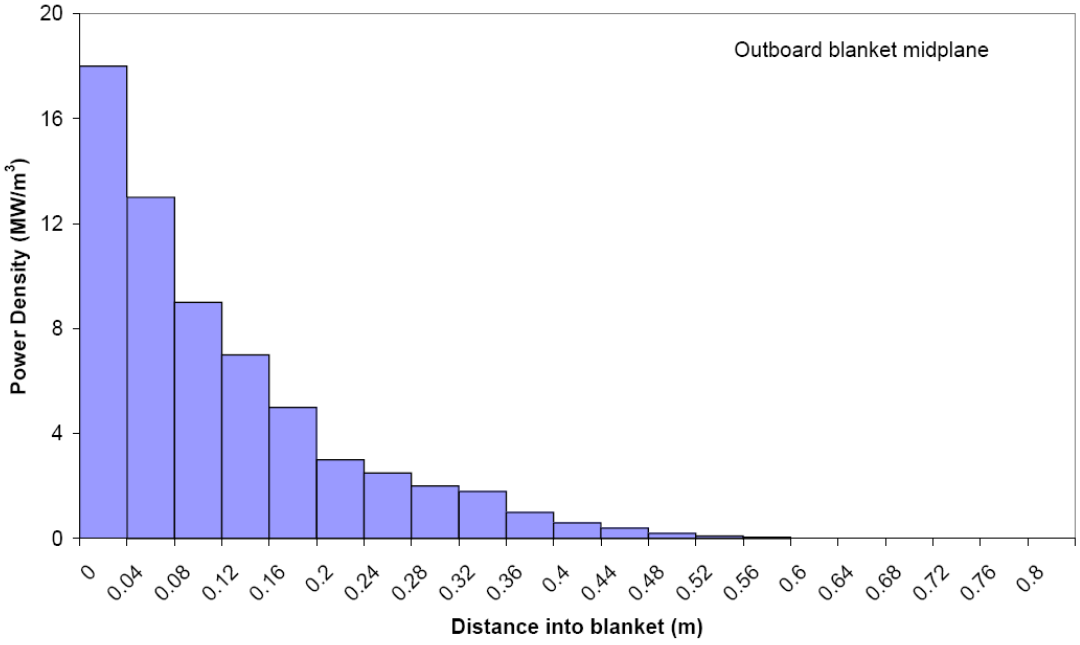

Power density deposited by neutrons varies rapidly as a function of distance from the first wall. Energy is mostly deposited in the first 30cm of the blanket away from the plasma.

S. Sato, K. Maki, Fus. Eng. Design **65** (2003) 501

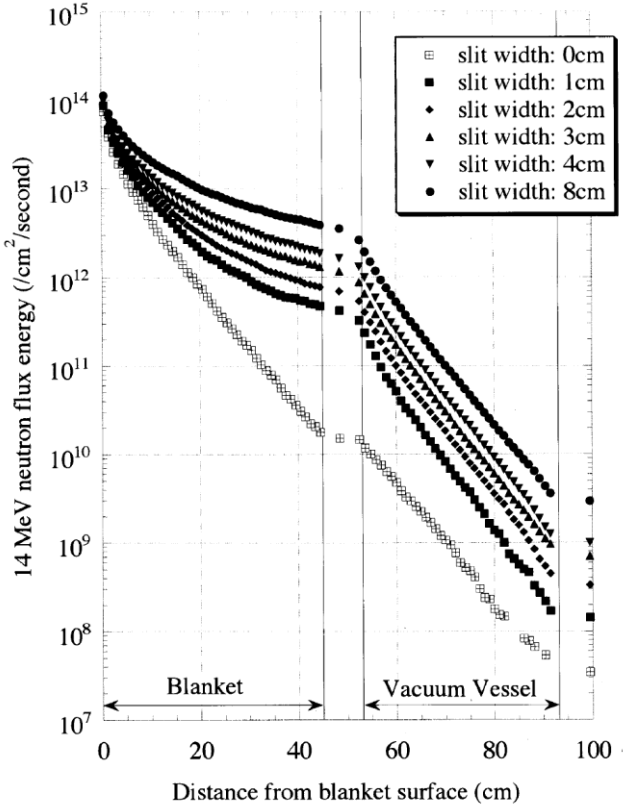

Fig. 2. Distributions of the 14 MeV neutron flux along the slit between the blanket modules under the neutron wall loading of 1 MW am^{-2}, the blanket thickness of 45 cm, the blanket composition of 80% SS and 20% water, the vacuum vessel thickness of 40 cm, and the vacuum vessel shield composition of 60% SS and 40% water.

Accurate predictive neutron transport calculations can now be performed using engineering design drawings as input.

UK Atomic Energy Authority

Reactor	Locations	Total flux (1/cm²/sec)	DPA/year (Eurofer)	He gas production (appm)	H gas production (appm)
DEMO	First Wall	3.79E+14	9.5	108.4	536.0
	blanket 1st layer	3.38E+14	7.8	82.8	415.4
	blanket middle	5.14E+13	1.0	8.6	44.4
	blanket 3rd layer	1.53E+11	2.4E-3	0.01	0.06
	back plate 1st layer	1.30E+11	1.8E-3	0.02	0.04
	back plate middle	4.10E+10	4.9E-4	0.01	0.01
ITER TBM	First Wall	1.86E+13	0.4	4.4	20.0
	side wall	8.53E+12	0.1	0.6	2.8
	back plate	1.14E+12	7.4E-3	0.1	0.1
PWR	core equivalent	1.64E+14	1.8	12.2	10.4
	core barrel	3.54E+13	0.3	3.0	1.5
	RPV average	3.50E+10	2.9E-4	9.6E-4	1.1E-3

Characteristic values of neutron flux, radiation damage and gas production at various locations in DEMO, ITER TBMs and PWR. ITER D-T model assumptions: 30000 deuterium-tritium shots, each lasting approximately 400s.

S. Zhang *et al.*, presentation at ICFRM16, Beijing, October 21-25, 2013.

UK Atomic Energy Authority

Computing stress and strain in reactor components due to exposure to irradiation

Deformations in the vicinity of a defect

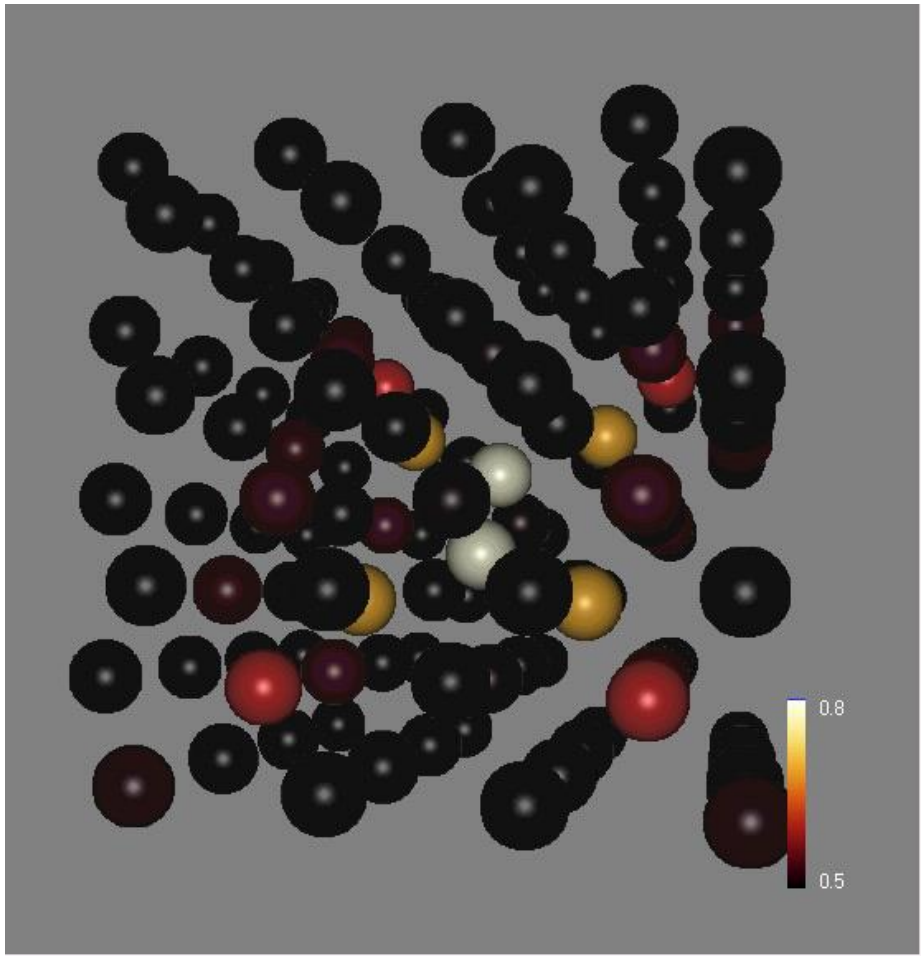

Lattice distortions in Fe near a self-interstitial atom defect. Lattice distortions in engineering are known as “strain”, related to “stress” (internal forces).

Elastic fields of defects

$$u_i(\mathbf{r}) = -P_{kl}\frac{\partial}{\partial x_l}G_{ik}(\mathbf{r}-\mathbf{R})$$

$$G_{ik}(\mathbf{r}) = \frac{1}{16\pi\mu(1-\nu)r}\left[(3-4\nu)\delta_{ik} + \frac{x_i x_k}{r^2}\right]$$

$$P_{ij} = -\int_{V_{\text{cell}}} \sigma_{ij}\,dV = -V_{\text{cell}}\overline{\sigma}_{ij}$$

Elements of the dipole tensor are almost always computed, as a by-product of almost any DFT or molecular statics simulation involving atomic relaxations.

E. Clouet *et al.*, Acta Mat. **56** (2008) 3450;
P.-W. Ma and S.L. Dudarev, Phys. Rev. Mat. **3** (2019) 013605

Elastic fields of defects

$$u_i(\mathbf{r}) = -P_{kl}\frac{\partial}{\partial x_l}G_{ik}(\mathbf{r}-\mathbf{R})$$

$$G_{ik}(\mathbf{r}) = \frac{1}{16\pi\mu(1-\nu)r}\left[(3-4\nu)\delta_{ik} + \frac{x_i x_k}{r^2}\right]$$

$$P_{ij} = -\int_{V_{\text{cell}}} \sigma_{ij}\,dV = -V_{\text{cell}}\overline{\sigma}_{ij}$$

$$P_{kl} = C_{klmn}\Omega_{mn}$$

relaxation volume tensor: the sum of its diagonal elements equals the relaxation volume (= "the volume") of the defect

P.-W. Ma and S.L. Dudarev, Phys. Rev. Mat. **3** (2019) 013605

Volumes of defects: literature data

UK Atomic Energy Authority

Theoretical values of the vacancy formation volume, V_F, in units of atomic volume, Ω, and the experimental data. 1 – estimates by Seeger [27] based on the activation volumes of self-diffusion, 2 – Jacucci and Taylor [107], 3 – Bauer et al. [108], 4 – Harder and Bacon [101], 5 – Ackland et al. [102], 6 – Rosato et al. [104], 7 – experimental data [109–111]

	V_F/Ω						
Metal	1	2	3	4	5	6	7
K		0.59–0.71[a]					
Na	0.25	0.65–0.72[a]					
Li	0.2–0.25	0.43–0.68[a]					
In	0.45						
Sn	0.25						
Cd	0.5						
Pb	0.4						
Zn	0.35–0.4						
Al	0.65						0.62[b]
Ag	0.75		0.69		0.78	0.76	
Au	0.65		0.63		0.73	0.72	0.52[c]
Cu	0.8		0.79		0.77	0.8	
Ni					0.88	0.8	
Pd						0.77	
Pt						0.76	0.7[d]
V				0.74			
Cr				0.84			
Ir						0.75	
Rh						0.77	
Nb				0.96			
Mo				0.73			
Ta				0.83			
W				0.68			

Y. Kraftmakher, Phys. Repts. **299** (1998) 79

Element	η	Interstitial relaxation	Vacancy relaxation
Al	7.54	1.86	−0.05
Cr	6.87	0.88	−0.27
Cu	7.20	1.45	−0.25
Fe	7.91	0.91	−0.32
Mo	9.66	0.85	−0.45
Nb	4.62	0.76	−0.41
Ni	8.21	1.85	−0.20
Ta	6.13	0.78	
V	4.90	0.77	
W	9.44	0.92	−0.28

W.G. Wolfer, J. Computer-Aided Mater. Des. **14** (2007) 403

Table 2
Results for Frenkel defects in Mo

P. Ehrhart, J. Nucl. Mater. **69 & 70** (1978) 200

Int. type	Anisotropy				$V_{1i}^{rel} = (\lambda_1+\lambda_2+\lambda_3)$ [at.vol.]	V_{1V}^{rel} [at.vol.]
	$\pi^{(2)}/\pi^{(1)}$	$\pi^{(3)}/\pi^{(1)}$	$\lambda_1-\lambda_2$	$\frac{1}{2}(\lambda_1+\lambda_2)-\lambda_3$		
⟨110⟩-split	0.05 ± 0.02	0.04 ± 0.02	(+) 1.1 ± 0.3	(+) 0.65 ± 0.2	1.1 ± 0.2	(−0.1)

Note the large variability of data: relaxation volumes are very difficult to measure accurately

Evaluation of dipole tensors and volumes of defects using DFT

UK Atomic Energy Authority

A general expression for elastic energy

$$E_D = \frac{1}{2}\int_V \sigma_{ij}(\mathbf{r})\epsilon_{ij}(\mathbf{r})dV$$

In the presence of small external strain, the following Taylor expansion applies:

$$E_D(\epsilon_{ij}^{ext}) = E_D(\epsilon_{ij}^{ext}=0) + \left(\frac{\delta E_D}{\delta \epsilon_{ij}^{ext}}\right)_{\epsilon_{ij}^{ext}=0} \epsilon_{ij}^{ext} + \cdots$$

Energy of interaction between a defect and external strain

$$E = -P_{ij}\epsilon_{ij}^{ext}$$

Hence the dipole tensor of a defect can be computed from the stress that it produces in a simulation cell (no volume relaxation)

$$P_{ij} = -\left(\frac{\delta E_D}{\delta \epsilon_{ij}^{ext}}\right)_{\epsilon_{ij}^{ext}=0} = -\int_V \sigma_{ij}^D dV$$

P.-W. Ma and S.L. Dudarev, Phys. Rev. Mat. **3** (2019) 013605

Evaluation of dipole tensors and volumes of defects using DFT

UK Atomic Energy Authority

Equations required for a numerical evaluation of the relaxation volume of a defect

$$E = -P_{ij}\epsilon_{ij}^{ext}$$

$$\Omega_{ij} = S_{ijkl}P_{kl}$$

$\mathbf{S} = \mathbf{C}^{-1}$ is the elastic compliance tensor

$$C_{ijkl}S_{klmn} = \frac{1}{2}(\delta_{im}\delta_{jn} + \delta_{in}\delta_{jm})$$

$$\Omega_{\mathrm{rel}} = Tr\Omega_{ij} = \Omega_{11} + \Omega_{22} + \Omega_{33}$$

P.-W. Ma and S.L. Dudarev, Phys. Rev. Mat. **3** (2019) 013605

Evaluation of dipole tensors and volumes of defects using DFT

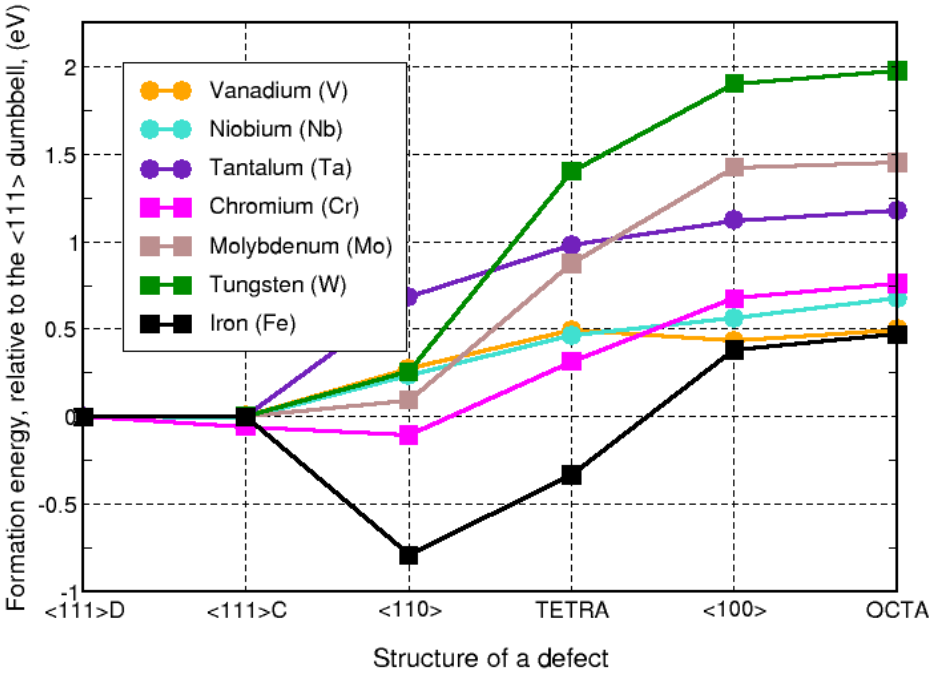

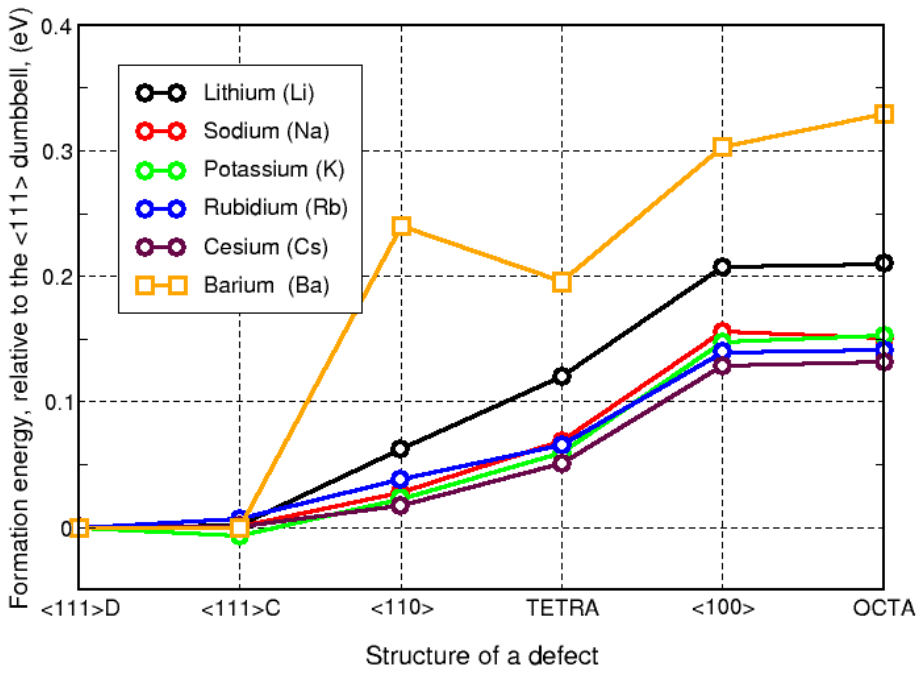

The universal character of defect structure in various bcc metals, apart from Fe, which stands out because of magnetism. In other bcc metals, including simple alkaline metals, the lowest energy SIA defect structure is a 111 crowdion.

P.-W. Ma and S.L. Dudarev, Phys. Rev. Mat. **3** (2019) 013605

Evaluation of dipole tensors and volumes of defects using DFT

UK Atomic Energy Authority

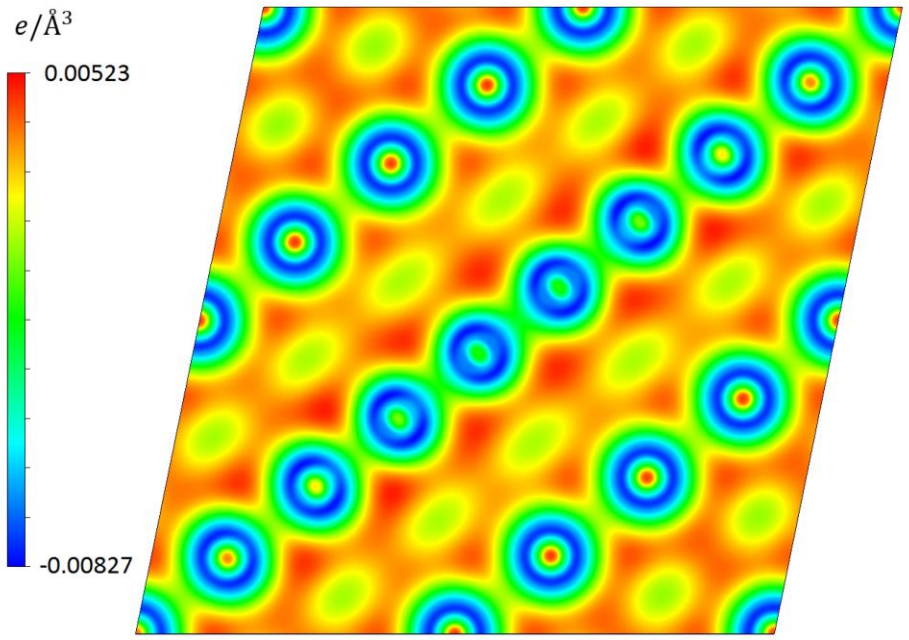

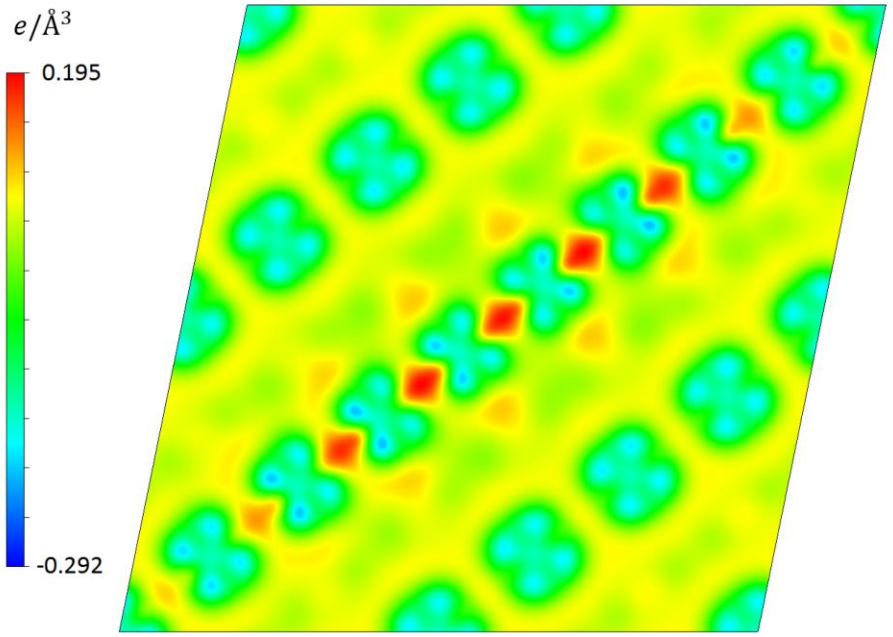

It is hard to offer a simple reason why the structure of a SIA defect appears universal for all the bcc metals. In sodium (left), the charge deformation associated with the defect is almost non-directional, whereas in tungsten (right), the effects of directional *d*-bonding are evident.

P.-W. Ma and S.L. Dudarev, Phys. Rev. Mat. **3** (2019) 013605

The symmetry-broken structure of an SIA defect in Cr, Mo and W

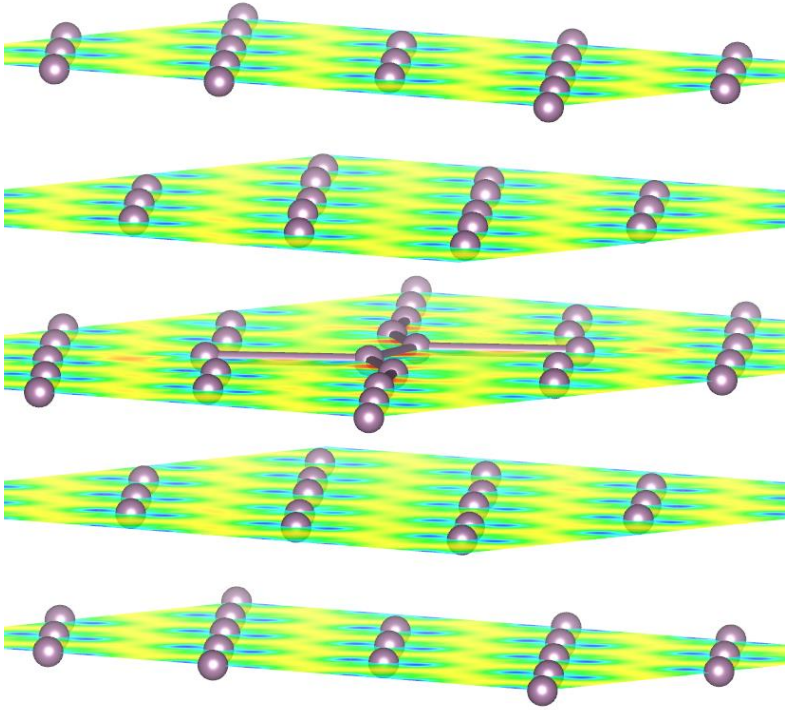

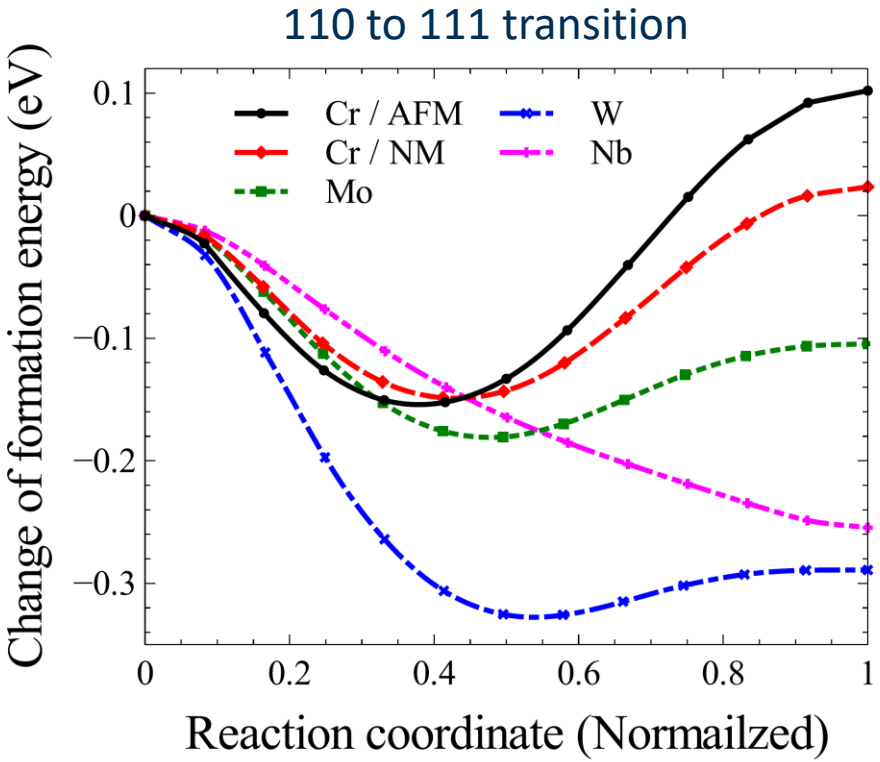

The structure of a symmetry-broken 111 self-interstitial atom defect in Cr, Mo and W. On average, the defect still migrates one-dimensionally. But symmetry breaking is responsible for the complex low temperature resistivity recovery stages in Cr, Mo and W. There is no symmetry-breaking in V, Nb, Ta.

P.-W. Ma and S.L. Dudarev, Phys. Rev. Mat. **3** (2019) 043606

Elastic dipoles and relaxation volumes of defects: direct DFT calculations

UK Atomic Energy Authority

TABLE XXIV. Elements of the dipole tensor P_{ij} (in eV units), the relaxation volume tensor Ω_{ij} (in Å^3 units), eigenvalues of the relaxation volume tensor $\Omega^{(i)}$ (in Å^3 units), and the relaxation volume of the defect Ω_{rel} (in atomic volume units Ω_0) computed for Fe.

Fe	P_{11}	P_{22}	P_{33}	P_{12}	P_{23}	P_{31}	Ω_{11}	Ω_{22}	Ω_{33}	Ω_{12}	Ω_{23}	Ω_{31}	$\Omega^{(1)}$	$\Omega^{(2)}$	$\Omega^{(3)}$	Ω_{rel}
⟨111⟩d	23.465	23.465	23.472	5.850	5.851	5.851	6.327	6.327	6.335	4.362	4.363	4.363	1.964	1.964	15.051	1.673
⟨111⟩c	23.186	23.186	23.193	5.903	5.904	5.904	6.252	6.252	6.259	4.402	4.402	4.402	1.850	1.850	15.056	1.653
⟨110⟩d	25.832	21.143	21.150	0.000	5.122	0.000	9.777	4.294	4.302	0.000	3.819	0.000	9.777	0.475	8.122	1.620
Tetra	21.396	23.331	23.339	0.000	0.001	0.000	4.607	6.871	6.880	0.000	0.000	0.000	4.607	6.871	6.880	1.619
⟨100⟩d	32.284	22.931	22.937	0.000	0.000	0.000	14.316	3.378	3.385	0.000	0.000	0.000	14.316	3.378	3.385	1.858
Octa	23.273	23.273	31.302	0.000	0.000	0.000	3.869	3.869	13.258	0.000	0.000	0.000	3.869	3.869	13.258	1.851
Vac	−3.081	−3.081	−3.081	0.000	0.000	0.000	−0.831	−0.831	−0.831	0.000	0.000	0.000	−0.831	−0.831	−0.831	−0.220

TABLE XX. Elements of the dipole tensor P_{ij} (in eV units), the relaxation volume tensor Ω_{ij} (in Å^3 units), eigenvalues of the relaxation volume tensor $\Omega^{(i)}$ (in Å^3 units), and the relaxation volume of the defect Ω_{rel} (in atomic volume units Ω_0) computed for W.

W	P_{11}	P_{22}	P_{33}	P_{12}	P_{23}	P_{31}	Ω_{11}	Ω_{22}	Ω_{33}	Ω_{12}	Ω_{23}	Ω_{31}	$\Omega^{(1)}$	$\Omega^{(2)}$	$\Omega^{(3)}$	Ω_{rel}
⟨111⟩d	52.754	52.754	52.754	13.128	13.128	13.128	9.209	9.209	9.209	7.402	7.402	7.402	1.808	1.808	24.012	1.712
⟨111⟩c	52.745	52.745	52.745	13.151	13.151	13.151	9.207	9.207	9.207	7.414	7.414	7.414	1.793	1.793	24.036	1.711
⟨110⟩d	56.960	52.557	52.557	0.000	11.277	0.000	10.908	8.693	8.693	0.000	6.358	0.000	10.908	2.335	15.050	1.753
Tetra	47.359	59.114	59.114	0.000	0.000	0.000	5.693	11.606	11.606	0.000	0.000	0.000	5.693	11.606	11.606	1.791
⟨100⟩d	65.920	53.379	53.379	0.000	0.000	0.000	14.254	7.945	7.945	0.000	0.000	0.000	14.254	7.945	7.945	1.868
Octa	52.741	52.741	67.209	0.000	0.000	0.000	7.623	7.623	14.901	0.000	0.000	0.000	7.623	7.623	14.901	1.868
Vac	−9.984	−9.984	−9.984	0.000	0.000	0.000	−1.743	−1.743	−1.743	0.000	0.000	0.000	−1.743	−1.743	−1.743	−0.324

P.-W. Ma and S.L. Dudarev, Phys. Rev. Mat. **3** (2019) 013605

Elastic dipoles and relaxation volumes of defects: direct DFT calculations

UK Atomic Energy Authority

TABLE VI. Elements of the dipole tensor P_{ij} (in eV units), the relaxation volume tensor Ω_{ij} (in Å^3 units), eigenvalues of the relaxation volume tensor $\Omega^{(i)}$ (in Å^3 units), and the relaxation volume of the defect $\Omega_{\rm rel}$ (in atomic volume units Ω_0) computed for Li.

Li	P_{11}	P_{22}	P_{33}	P_{12}	P_{23}	P_{31}	Ω_{11}	Ω_{22}	Ω_{33}	Ω_{12}	Ω_{23}	Ω_{31}	$\Omega^{(1)}$	$\Omega^{(2)}$	$\Omega^{(3)}$	$\Omega_{\rm rel}$
⟨111⟩d	2.071	2.071	2.071	0.796	0.796	0.796	7.930	7.930	7.930	5.577	5.577	5.577	2.353	2.353	19.084	1.175
⟨111⟩c	2.063	2.063	2.063	0.761	0.761	0.761	7.899	7.899	7.899	5.334	5.334	5.334	2.566	2.566	18.567	1.171
⟨110⟩d	2.109	2.188	2.188	0.000	0.727	0.000	6.936	8.947	8.947	0.000	5.096	0.000	6.936	3.851	14.043	1.227
Tetra	2.196	2.160	2.160	0.000	0.000	0.000	8.923	8.011	8.011	0.000	0.000	0.000	8.923	8.011	8.011	1.232
⟨100⟩d	2.764	1.911	1.911	0.000	0.000	0.000	22.893	1.164	1.164	0.000	0.000	0.000	22.893	1.164	1.164	1.246
Octa	1.898	1.898	2.754	0.000	0.000	0.000	1.094	1.094	22.892	0.000	0.000	0.000	1.094	1.094	22.892	1.239
Vac	−0.937	−0.937	−0.937	0.000	0.000	0.000	−3.589	−3.589	−3.589	0.000	0.000	0.000	−3.589	−3.589	−3.589	−0.532

TABLE XVI. Elements of the dipole tensor P_{ij} (in eV units), the relaxation volume tensor Ω_{ij} (in Å^3 units), eigenvalues of the relaxation volume tensor $\Omega^{(i)}$ (in Å^3 units), and the relaxation volume of the defect $\Omega_{\rm rel}$ (in atomic volume units Ω_0) computed for Mo.

Mo	P_{11}	P_{22}	P_{33}	P_{12}	P_{23}	P_{31}	Ω_{11}	Ω_{22}	Ω_{33}	Ω_{12}	Ω_{23}	Ω_{31}	$\Omega^{(1)}$	$\Omega^{(2)}$	$\Omega^{(3)}$	$\Omega_{\rm rel}$
⟨111⟩d	39.601	39.601	39.601	7.609	7.609	7.609	8.087	8.087	8.087	6.113	6.113	6.113	1.975	1.975	20.313	1.538
⟨111⟩c	39.597	39.597	39.597	7.599	7.599	7.599	8.087	8.087	8.087	6.105	6.105	6.105	1.982	1.982	20.297	1.538
⟨110⟩d	42.470	39.944	39.944	0.000	6.757	0.000	9.196	7.896	7.896	0.000	5.429	0.000	9.196	2.468	13.325	1.584
Tetra	37.531	43.685	43.685	0.000	0.000	0.000	6.391	9.558	9.558	0.000	0.000	0.000	6.391	9.558	9.558	1.617
⟨100⟩d	48.989	40.370	40.370	0.000	0.000	0.000	11.788	7.353	7.353	0.000	0.000	0.000	11.788	7.353	7.353	1.680
Octa	39.601	39.601	50.174	0.000	0.000	0.000	6.994	6.994	12.435	0.000	0.000	0.000	6.994	6.994	12.435	1.675
Vac	−9.576	−9.576	−9.576	0.000	0.000	0.000	−1.956	−1.956	−1.956	0.000	0.000	0.000	−1.956	−1.956	−1.956	−0.372

P.-W. Ma and S.L. Dudarev, Phys. Rev. Mat. **3** (2019) 013605

Effects of symmetry

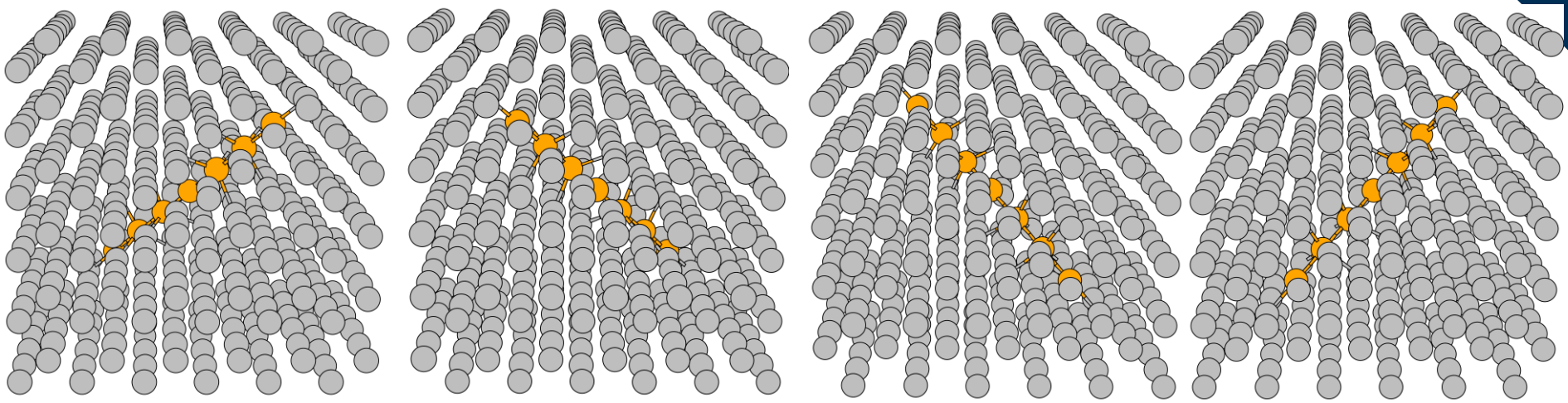

$$\begin{pmatrix} P_a & P_b & P_b \\ P_b & P_a & P_b \\ P_b & P_b & P_a \end{pmatrix} \quad \begin{pmatrix} P_a & -P_b & P_b \\ -P_b & P_a & -P_b \\ P_b & -P_b & P_a \end{pmatrix} \quad \begin{pmatrix} P_a & P_b & -P_b \\ P_b & P_a & -P_b \\ -P_b & -P_b & P_a \end{pmatrix} \quad \begin{pmatrix} P_a & -P_b & -P_b \\ -P_b & P_a & P_b \\ -P_b & P_b & P_a \end{pmatrix}$$

Averaging over orientations of the defect produces a diagonal tensor

$$\begin{pmatrix} P_a & 0 & 0 \\ 0 & P_a & 0 \\ 0 & 0 & P_a \end{pmatrix} = P_a \delta_{ij}$$

Strain field of defects

In applications, we are interested in the elastic field produced by many defects => self-averaging

$$\langle \Omega_{mn} \rangle = \sum_{s=1}^{3} \Omega^{(s)} \langle e_m^{(s)} e_n^{(s)} \rangle$$

$$\langle \Omega_{mn} \rangle = \frac{1}{3} \Omega_{\mathrm{rel}} \delta_{mn}$$

Anisotropic crystallographic effects are not significant for large structural components, since grain orientations are random

strain

$$\epsilon_{ij}(\mathbf{r}) = \frac{1}{4\pi} \frac{1+\nu}{1-\nu} \int \frac{\omega_{\mathrm{rel}}(\mathbf{R})}{|\mathbf{r}-\mathbf{R}|^3} \left(\frac{1}{3}\delta_{ij} - \eta_i \eta_j \right) \mathrm{d}^3 R$$

$$\eta_i = \frac{(\mathbf{r}-\mathbf{R})_i}{|\mathbf{r}-\mathbf{R}|}$$

$$\omega_{\mathrm{rel}}(\mathbf{r}) = \sum_a \Omega_{\mathrm{rel}}^{(a)} \delta(\mathbf{r} - \mathbf{R}_\alpha)$$

dimensionless

$\omega(\mathbf{r})$ is the density of relaxation volumes of defects.

Macroscopic stress from defects

UK Atomic Energy Authority

$$\epsilon_{ij}(\mathbf{r}) = \frac{1}{4\pi}\frac{1+\nu}{1-\nu}\int \frac{\omega_{\mathrm{rel}}(\mathbf{R})}{|\mathbf{r}-\mathbf{R}|^3}\left(\frac{1}{3}\delta_{ij} - \eta_i\eta_j\right)\mathrm{d}^3R.$$

$$\epsilon_{ij}(\mathbf{r}) = -\frac{1}{12\pi}\frac{1+\nu}{1-\nu}\int \omega_{\mathrm{rel}}(\mathbf{R})\frac{\partial^2}{\partial x_i \partial x_j}\frac{1}{|\mathbf{r}-\mathbf{R}|}\mathrm{d}^3R.$$

The above two equations for strain are fully equivalent. Now we evaluate stress

$$\begin{aligned}\sigma_{ij}(\mathbf{r}) = &-\frac{\mu}{6\pi}\frac{1+\nu}{1-\nu}\int \omega_{\mathrm{rel}}(\mathbf{R})\frac{\partial^2}{\partial x_i \partial x_j}\frac{1}{|\mathbf{r}-\mathbf{R}|}\mathrm{d}^3R \\ &-\frac{\mu}{12\pi}\left(\frac{1+\nu}{1-\nu}\right)\left(\frac{2\nu}{1-2\nu}\right)\delta_{ij} \\ &\times\sum_k \int \omega_{\mathrm{rel}}(\mathbf{R})\frac{\partial^2}{\partial x_k^2}\frac{1}{|\mathbf{r}-\mathbf{R}|}\mathrm{d}^3R,\end{aligned}$$

The second term is the contribution from the (singular!) core of the defect:

$$\sum_k \frac{\partial^2}{\partial x_k^2}\frac{1}{|\mathbf{r}-\mathbf{R}|} = \Delta\frac{1}{|\mathbf{r}-\mathbf{R}|} = -4\pi\delta(\mathbf{r}-\mathbf{R})$$

Macroscopic stress from defects

UK Atomic Energy Authority

$$\sigma_{ij}(\mathbf{r}) = -\frac{\mu}{6\pi}\frac{1+\nu}{1-\nu}\int \omega_{\mathrm{rel}}(\mathbf{R})\frac{\partial^2}{\partial x_i \partial x_j}\frac{1}{|\mathbf{r}-\mathbf{R}|}\mathrm{d}^3R. + \frac{\mu}{3}\left(\frac{1+\nu}{1-\nu}\right)\left(\frac{2\nu}{1-2\nu}\right)\delta_{ij}\omega_{\mathrm{rel}}(\mathbf{r}).$$

The total stress field generated by a distribution of defects. The density of body forces equals

$$f_i(\mathbf{r}) = -\frac{\partial \sigma_{ij}(\mathbf{r})}{\partial x_j} = \frac{2\mu}{3}\left(\frac{1+\nu}{1-\nu}\right)\frac{\partial}{\partial x_i}\omega_{\mathrm{rel}}(\mathbf{r}) - \frac{\mu}{3}\left(\frac{1+\nu}{1-\nu}\right)\left(\frac{2\nu}{1-2\nu}\right)\frac{\partial}{\partial x_i}\omega_{\mathrm{rel}}(\mathbf{r}).$$

$$\frac{\partial}{\partial x_j}\sigma_{ij}(\mathbf{r}) + f_i(\mathbf{r}) = 0 \qquad f_i(\mathbf{r}) = -B\frac{\partial}{\partial x_i}\omega_{\mathrm{rel}}(\mathbf{r})$$

where $B = 2\mu(1+\nu)/[3(1-2\nu)]$ is the bulk modulus

Condition of mechanical equilibrium

A full condition of equilibrium includes gravity, thermal expansion, *and* swelling due to defects

$$\frac{\partial \sigma_{ik}(\mathbf{r})}{\partial x_k} + \rho g_i - B\alpha \frac{\partial T}{\partial x_i} - B \frac{\partial}{\partial x_i} \omega_{rel}(\mathbf{r}) = 0.$$

gravity

thermal expansion

defects

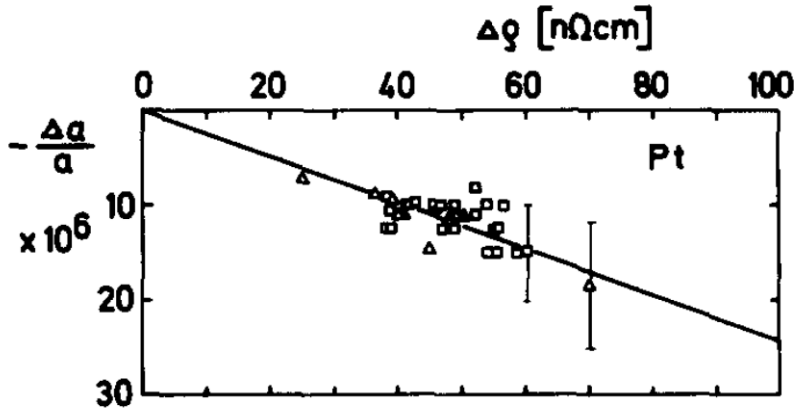

Fig. 1. Lattice parameter versus resistivity change after quenching of Pt. (Δ(333/511), □ (422) X-ray reflection).

$$\left(\frac{\Delta v}{v}\Big/\Delta\rho\right)_v^{Pt} = -(0.72 \pm 0.09) \times 10^3\ (\Omega\,\mathrm{cm})^{-1}$$

Defects, as opposed to temperature, generate compressive or tensile strains: this agrees with DFT – vacancies give rise to lattice contraction

W. Hertz *et al.*, Phys. Letters **43A** (1973) 289

Volumes of all the possible defects

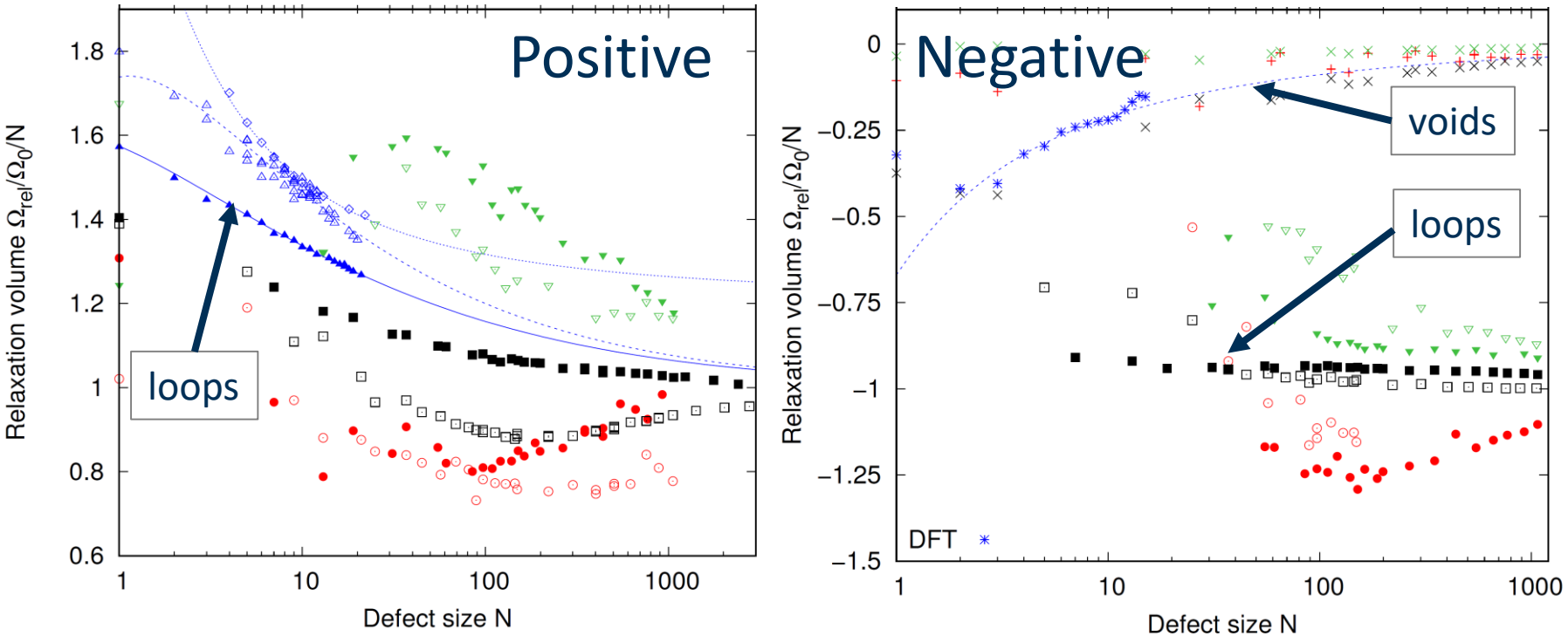

Relaxation volumes of (left) self-interstitial and (right) vacancy defects. The smallest defects produce the largest stresses and deformations per defect. The dominant contribution to stress in irradiated reactor components is from the smallest dislocation loops. Voids produce almost no stress.

D. R. Mason *et al.*, J. Appl. Phys. **126**, 075112 (2019)

Stress field produced by a cascade event

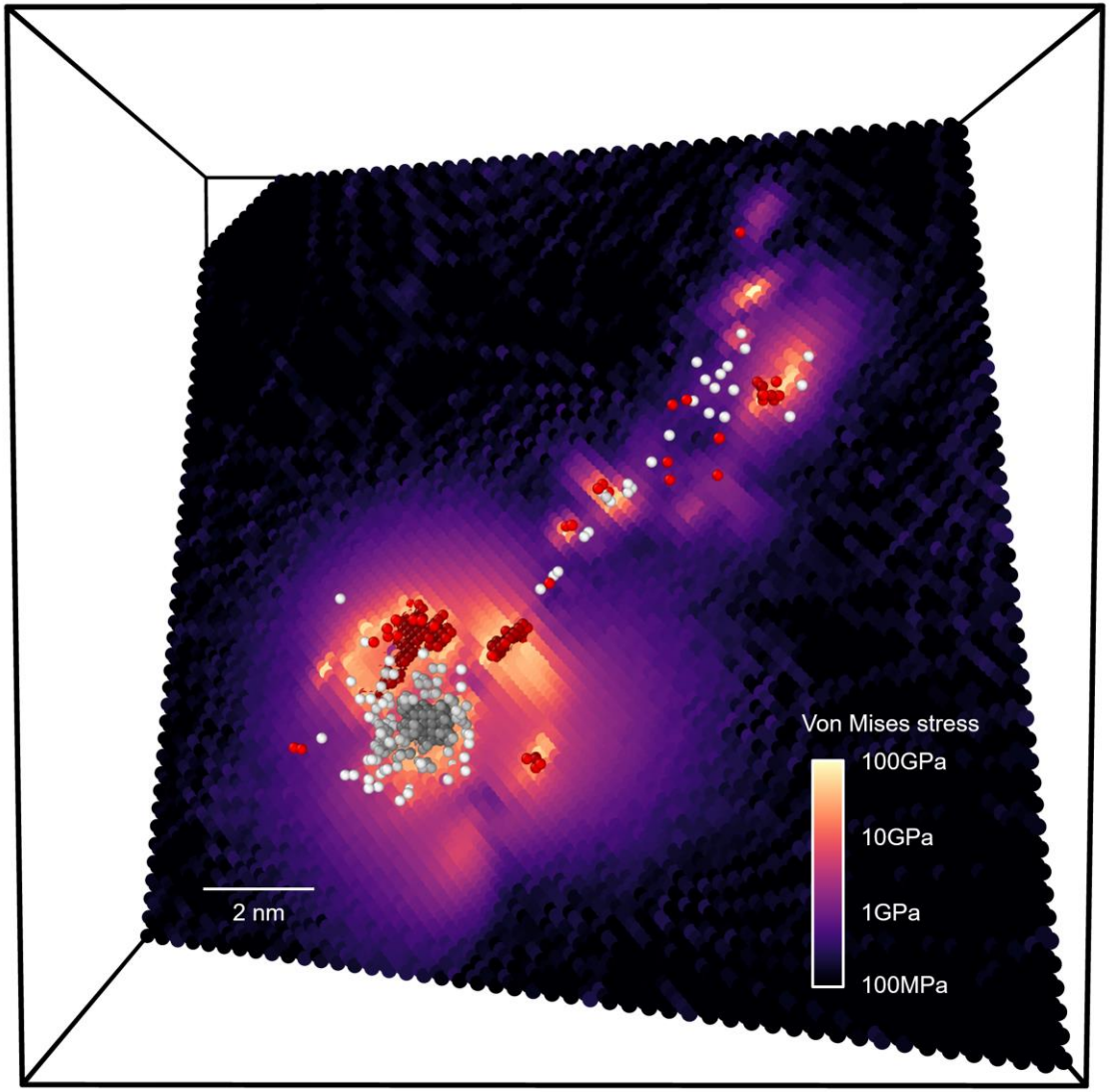

D. R. Mason *et al.,* J. Appl. Phys. **126** (2019) 075112

Stress field produced by a cascade event

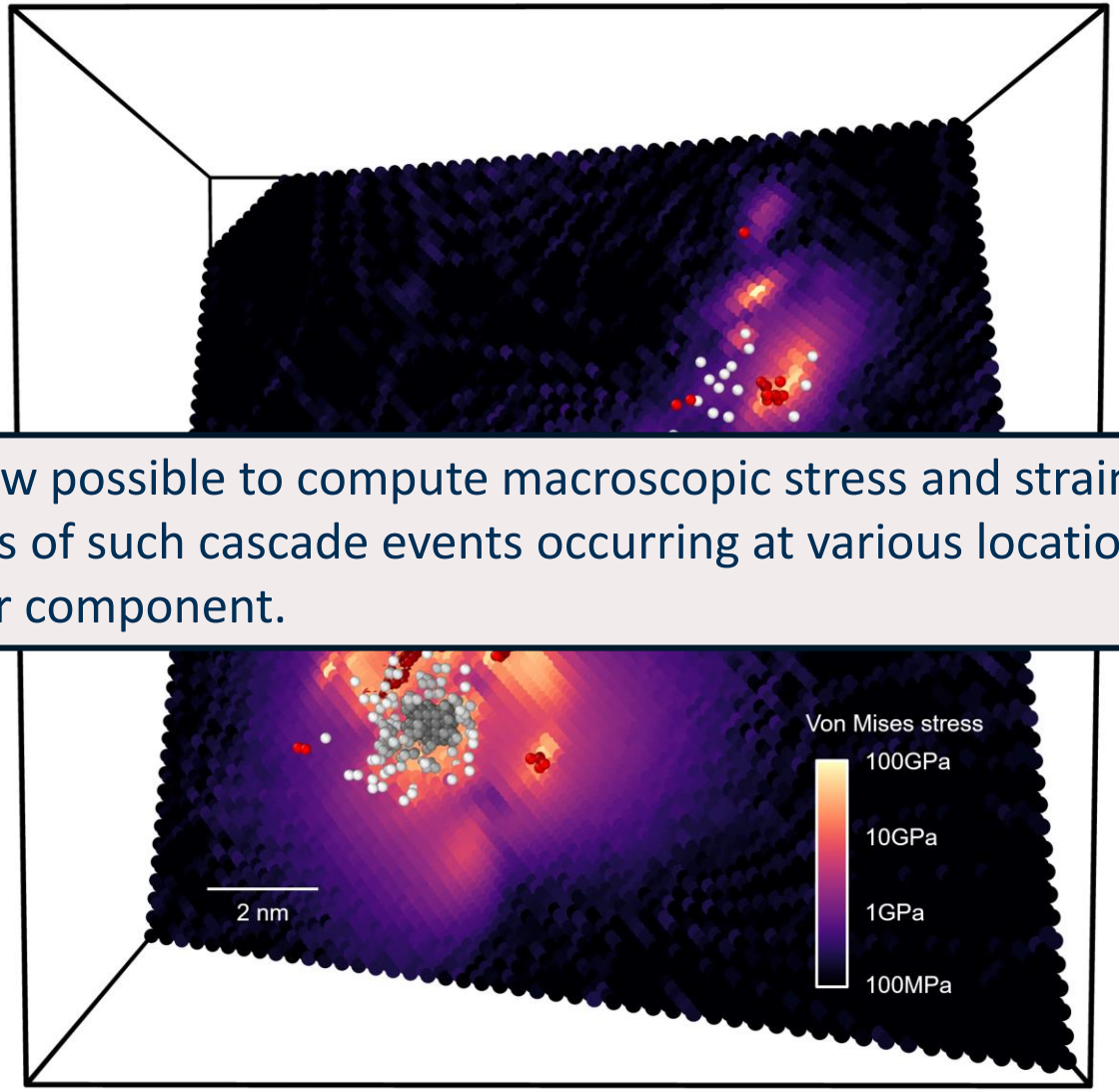

It is now possible to compute macroscopic stress and strain from trillions of such cascade events occurring at various locations in a reactor component.

D. R. Mason *et al.,* J. Appl. Phys. **126** (2019) 075112

A case study: stress in an irradiated spherical shell

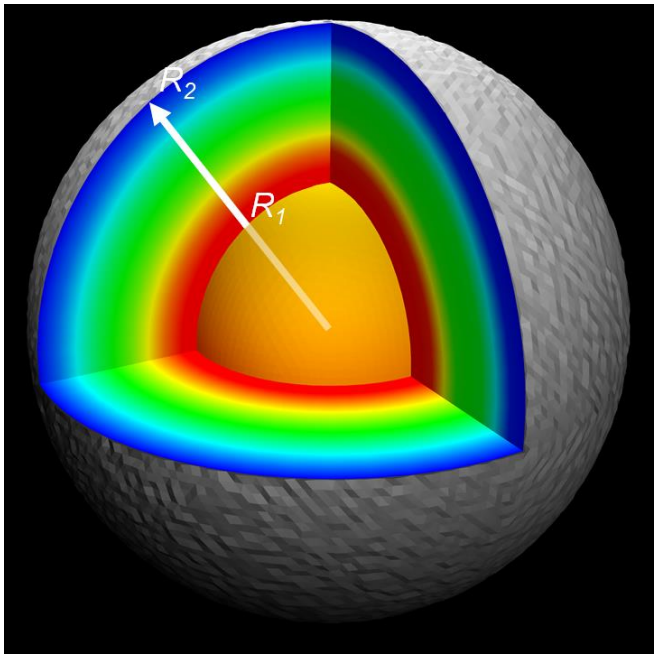

A steel shell containing a volumetric neutron source.

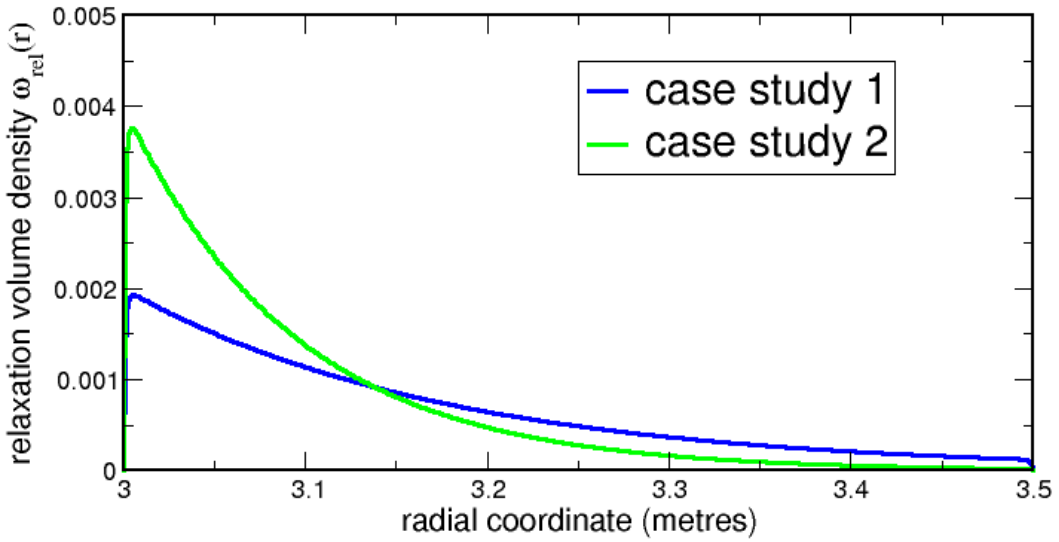

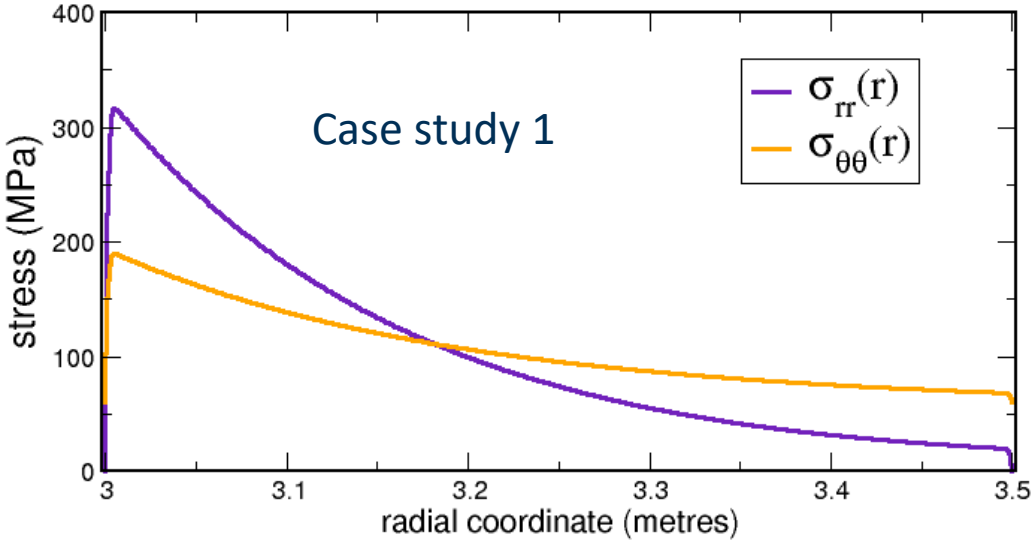

Nucl. Fusion **58** (2018) 126002

UK Atomic Energy Authority

Summary

Modelling radiation effects in materials, used in combination with high resolution *ex*- and *in-situ* experimental techniques, is progressing, facilitating new opportunities in engineering design.

Direct “mechanistic” approach, involving both the incremental development of established models (advanced DFT, machine learning potential-based MD) and fundamentally new mathematical algorithms, delivers steadily improving predictions.

Simulations of cascade events, and databases of defect structures produced in such events – including radiation damage events in microstructurally complex materials – provides the information critically significant for the development of microstructurally complex materials for advanced nuclear applications.